

Changing the circuit-depth complexity of measurement-based quantum computation with hypergraph states

Mariami Gachechiladze,¹ Otfried Gühne,¹ and Akimasa Miyake²

¹*Naturwissenschaftlich-Technische Fakultät, Universität Siegen, 57068 Siegen, Germany*

²*Center for Quantum Information and Control, Department of Physics and Astronomy, University of New Mexico, Albuquerque, NM 87131, USA*

(Dated: December 14, 2024)

The circuit model of quantum computation defines its logical depth or “computational time” in terms of temporal gate sequences, but the measurement-based model could allow totally different time ordering and parallelization of logical gates. We introduce a deterministic scheme of universal measurement-based computation, using only Pauli measurements on multi-qubit hypergraph states generated by the Controlled-Controlled-Z (CCZ) gates. In contrast to the cluster-state scheme where the Clifford gates are parallelizable, our scheme enjoys massive parallelization of CCZ and $SWAP$ gates, so that the computational depth grows with the number of global applications of Hadamard gates, or, in other words, with the number of changing computational bases. An exponentially-short depth implementation of an N -times Controlled-Z gate illustrates a novel trade-off between space and time complexity.

Introduction.— A typical way to build a computer, classical or quantum, is to first realize a certain set of elementary gates which can then be combined to perform algorithms. The set of gates is called universal if arbitrary algorithms can be implemented. Consequently, the concept of universality is fundamental in computer science. While the most common choice for the universal gate set in quantum circuits is a two-qubit entangling gate supplemented by certain single-qubit gates [1], the universal gate set given by the three-qubit Toffoli gate [or the Controlled-Controlled-Z (CCZ) gate for our case] and the one-qubit Hadamard (H) gate [2, 3] is fascinating for several reasons.

First, the Toffoli gate alone is already universal for reversible classical computation. Consequently, the set may give insight into fundamental questions about the origin of quantum computational advantage, in the sense that changing the bases among complementary observables (by the Hadamard gates) brings power to quantum computation [4–8]. Second, this gate set allows certain transversal implementations of fault-tolerant universal quantum computation using topological error correction codes. Transversality means that, in order to perform gates on the encoded logical qubits, one can apply corresponding gates to the physical qubits in a parallel fashion, and this convenience has sparked recent interest on this gate set [9–14]. Third, the many-body entangled states generated by the CCZ gates are known as hypergraph states in entanglement theory [15–19]. They found applications in quantum algorithms [20] and Bell inequalities [21]. Furthermore, as discussed below, they were recently utilized in measurement-based quantum computation (MBQC) [22, 23], because they overlap with renormalization-group fixed-point states of 2D symmetry-protected topological orders with global \mathbb{Z}_2 symmetry [24].

Motivated by these observations, we introduce a

scheme of MBQC for the gate set of $\{CCZ, H\}$, using multi-qubit hypergraph states. MBQC is a scheme of quantum computation where first a highly-entangled multi-particle state is created as a resource, then the computation is carried out by performing local measurements on the particles only [25, 26]. Compared with the canonical model of MBQC using cluster states [27] generated by Controlled-Z (CZ) gates, our scheme allows to extend substantially several key aspects of MBQC, such as the set of parallelizable gates and the byproduct group to compensate randomness of measurement outcomes (see [28–30] for previous extensions using tensor network states). Although 2D ground states with certain symmetry-protected topological orders have been shown to be universal for MBQC [22, 23], our construction has a remarkable feature that it allows *deterministic* MBQC, where the layout of a simulated quantum circuit can be predetermined.

As a major application, we identify a systematic way to implement an N -qubit generalized Controlled-Z ($C^N Z$) gate, a key logical gate for quantum algorithms such as the unstructured database search [31], in a depth logarithmic in N . This is an *exponential* reduction compared to a conventional implementation [32], although recently a comparable decomposition has been proposed in a different context of Hamiltonian engineering [33]. In this way, our scheme might shed new light on near-term noisy quantum computation where limited computational time seems to be the bottleneck. Finally, note that the required elementary three-qubit gate is more challenging in practice, but its implementation has been demonstrated in various platforms [34–36].

Summary of the computational scheme.— In MBQC, an algorithm is executed by performing local measurements on some entangled resource state. Consequently, two different physical resources, the entangling gates needed to prepare the state and the required class of mea-

	Cluster State	Hypergraph State
Preparation gates	$CZ \in \mathcal{C}_2$	$CCZ \in \mathcal{C}_3$
Measurements	Pauli + \mathcal{C}_2	Pauli
Implemented gates	\downarrow \mathcal{C}_2 \downarrow \mathcal{C}_3	\downarrow CCZ, H
Byproduct	$\{X, Z\}$	$\{CZ, X, Z\}$
Parallelized gates	\mathcal{C}_2	$\{CCZ^{nn}, SWAP\}$

TABLE I. Features of MBQC schemes using cluster and hypergraph states. Our scheme with a hypergraph state implements all logical CCZ and $SWAP$ gates without adaptation of measurements, leading to a massive parallelization of these.

measurements, characterize the MBQC scheme. To provide a fine-grained classification, let us define the Clifford hierarchy of unitary gates [37]. The unitary gates in the k -th level of the Clifford hierarchy \mathcal{C}_k are defined inductively, with \mathcal{C}_1 consisting of tensor products of Pauli operators, and $\mathcal{C}_{k+1} = \{U | \forall P \in \mathcal{C}_1, UPU^\dagger \in \mathcal{C}_k\}$. The gates in \mathcal{C}_2 form the so-called Clifford group, preserving the Pauli group operators under conjugation. They allow an efficient classical simulation if the initialization and read-out measurements are performed in the Pauli bases [38].

In order to discuss the complexity of MBQC, one needs to consider three aspects. The first is the adaptation of measurement bases, namely whether the choice of some measurement bases should depend on the results of previous measurements. Second, this naturally induces the notion of parallelism and logical depth (cf. [39, 40]). Some classes of gates can be carried out by simultaneous measurements, but for implementing other gates one needs to adapt the measurement bases, increasing the logical depth of an underlying circuit. Third, due to intrinsic randomness in the measurement outcomes, there are always byproduct operators needed to be corrected, in order to make MBQC deterministic. While it is known that the correction of Pauli operators can be accumulated to the end of computation by classical feed-forwarding of measurement outcomes, one may need to adapt measurement bases and perform additional gates in general. This step is referred to as a correction step.

In the canonical scheme of MBQC using the cluster state, Pauli measurements implement Clifford gates in \mathcal{C}_2 without any adaptation of measurement bases, so these gates can be parallelized. As Clifford gates are not universal, more general measurements in the X - Y -plane of the Bloch sphere must be performed to generate unitaries in \mathcal{C}_3 . The byproduct group is generated by the Pauli operators X and Z .

Our scheme, however, has several key differences summarized in Table I. Our state is prepared using CCZ gates (note that $CCZ \in \mathcal{C}_3$), but Pauli measurements alone are sufficient for universal computation. We choose $\{CCZ, H\}$ to be the logical gate set for universal computation. Indeed, we can implement all logical CCZ gates at *arbitrary* distance in parallel, by showing that nearest neighbor CCZ gates (CCZ^{nn}) and $SWAP$ gates are ap-

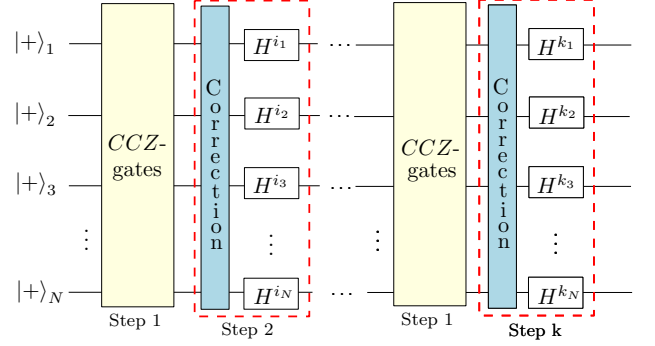


FIG. 1. Any quantum computation can be described as alternative applications of logical CCZ and Hadamard gates. Our MBQC scheme allows a parallelization where all logical CCZ (namely, CCZ^{nn} and $SWAP$) gates are implemented first simultaneously, and each Hadamard layer, which requires adaptation of measurement bases to correct prior byproduct operators, increases the quantum computation depth by one.

plicable without adaptation although they do not commute as unitary gates. Our implementation generates the group of byproduct operators $\{CZ, X, Z\}$, which differs from the standard byproduct group. Since we need Hadamard gates to achieve universality and our byproduct group is not closed under the conjugation with the Hadamard gate, we need to correct all CZ byproducts before the Hadamard gates. Thus, the logical depth grows according to the number of global applications of Hadamard gates, effectively changing the computational bases (see Fig. 1).

Hypergraph states and measurement rules.— Hypergraph states are generalizations of multi-qubit graph states. A hypergraph state corresponds to a hypergraph $H = (V, E)$, where V is a set of vertices (corresponding to the qubits) and E is a set of hyperedges, which may connect more than two vertices (see Fig. 2 for an example). The hyperedges correspond to interactions required for the generation of the state, as the state is defined as

$$|H\rangle = \prod_{e \in E} C_e |+\rangle^{\otimes |V|}, \quad (1)$$

where the C_e 's are generalized CZ gates, $C_e = \mathbb{1} - 2|1 \dots 1\rangle\langle 1 \dots 1|$ acting on the Hilbert space associated to $|e|$ qubits and $|+\rangle$ is a single-qubit eigenstate of the Pauli- X observable. Hypergraph states created by only three-qubit CCZ gates are called three-uniform.

Usually in MBQC protocols CZ gates are used as they guarantee information flow via perfect teleportation [26, 27]. For three-uniform hypergraph states, however, Pauli- Z measurements give CZ gates only probabilistically. But using a novel non-trivial Pauli- X measurement rule, we will achieve deterministic teleportation via projecting on CZ gates with unit probability. Later we show that the CCZ gates for the generation of the states can also be used in computation as logical CCZ gates

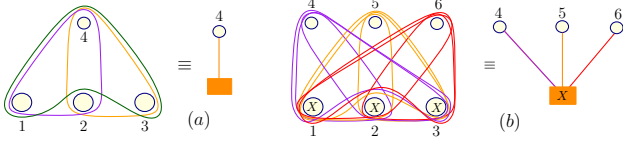


FIG. 2. (a) Denoting the four-qubit hypergraph state with hyperedges $E = \{\{1, 2, 4\}, \{2, 3, 4\}, \{1, 3, 4\}\}$ with the vertex and the box. (b) Pauli-X measurements on vertices 1, 2, 3 by Pauli-X measurement on the box.

with certainty. This finally guarantees determinism of our protocol.

Pauli measurements on a graph state always project onto a graph state, up to local unitary transformations [41]. For hypergraph states only the Pauli-Z measurement rule is known [17] and Pauli-X measurements lead, in general, out of the hypergraph state space. In the Appendix, we give a sufficient criterion and a rule for Pauli-X measurements to map hypergraph states to hypergraph states. This rule is our technical invention here, and entirely covers the known graph state Pauli-X measurement rule.

For simplicity we use the following notation: Given vertices $V = \{1, 2, 3\}$, if every two out of those three vertices are in a three-qubit hyperedge with a vertex $k \geq 4$, we draw a box instead of these three vertices and connect it with an edge to the vertex k [see Fig. 2 (a)]. In addition, we say that a box is measured in the \mathcal{M} -basis if all three qubits $\{1, 2, 3\}$ are measured in the \mathcal{M} -basis [see Fig. 2 (b), where $\mathcal{M} = X$]. Now we can formulate the main two examples of measurement rules needed for our concept of MBQC: In Fig. 3 (a) and (b) the post-measurement states are graph states with unit probability. By direct inspection one can check that there are only two possible local Clifford equivalent post-measurement states when $\mathcal{M} = X$.

Universal resource state and MBQC scheme.— Now we present our protocol for deterministic MBQC:

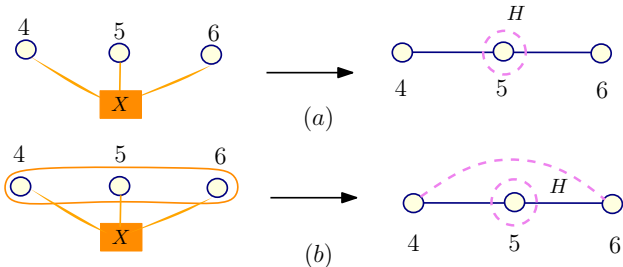


FIG. 3. Pauli-X-measurements on the given hypergraph states result in graph states, with a Hadamard gate applied to its vertex 5. All dashed lines (depicting byproducts) appear additionally if the product of measurement outcomes on vertices 1, 2, 3 is -1 . (a) Pauli-Z byproduct. (b) Pauli-Z and CZ byproducts.

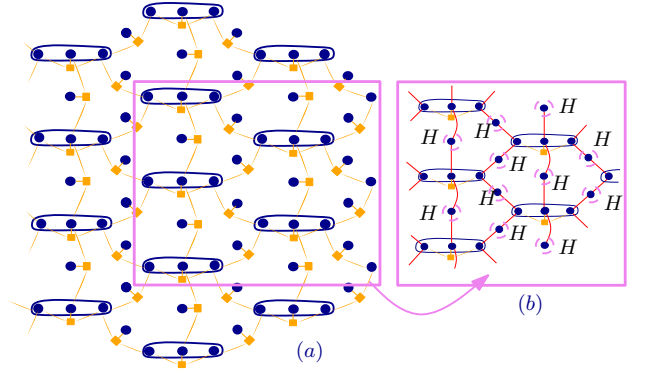


FIG. 4. (a) The universal resource state composed of elements on Fig. 3 (a) and (b). (b) Post-measurement state obtained after measuring all boxes in Pauli-X bases, except the ones attached to three qubits surrounded by a hyperedge. All dashed circles represent Pauli-Z byproducts.

Theorem 1. *Consider the three-uniform hypergraph state made by interactions as in Fig. 4. It enables universal and deterministic MBQC using Pauli measurements only. All logical CCZ gates over arbitrary distance can be implemented in parallel, adaptivity of measurements is required only for each logical Hadamard gate layer.*

For universality we demonstrate that we can implement the logical CCZ and H gates via Pauli measurements. Note that we have to secure independently three inputs and three outputs in of an CCZ hyperedge in a hypergraph state to be used as a *logical CCZ* gate. We realize the CCZ gate on arbitrary qubits in two steps: a nearest neighbor CCZ gate (CCZ^{nn}) and a $SWAP$ gate, swapping an order of inputs. In our discussion we assume that information flows from the bottom to the top.

We start by measuring all boxes in the X basis, except the ones attached to three vertices surrounded by a hyperedge CCZ . As a result we get graph edges connecting different parts of the new state, see the transition from Fig. 4 (a) to (b). We use the resource in Fig. 5 to implement the CCZ^{nn} gate. The box is measured in the Pauli-Z basis and just gets removed. The three vertices to which the box was attached to are still surrounded a hyperedge CCZ and additionally have local Pauli-Z byproducts. These three qubits are connected to the rest

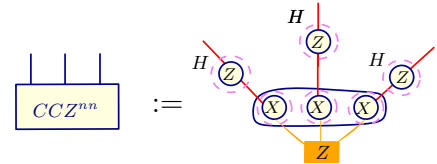


FIG. 5. A nearest-neighbor CCZ gate is implemented up to $\{Z, CZ\}$ byproducts. The CZ byproducts are not shown here, they appear between any two of the three vertices. See the Appendix for details.

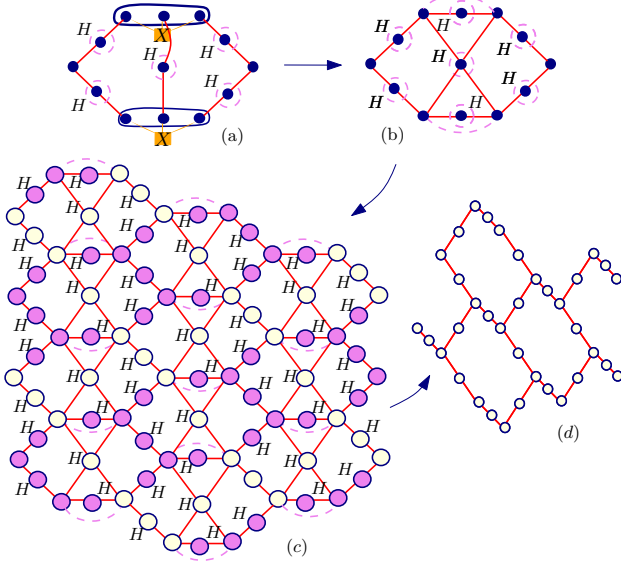


FIG. 6. Measuring all the boxes as in (a) gets rid of hyperedges entirely and projects on the graph state with Pauli- Z and CZ byproducts depicted by dashed lines in (b). The hexagonal lattice (d) is obtained deterministically after measuring colored vertices in suitable Pauli bases on (c).

of the state with the graph edges, and performing measurements as shown on Fig. 5 teleports the CCZ gate to the output qubits (up to $\{CZ, Z\}$ byproducts). See Fig. 9 in the Appendix for the explicit derivation.

Now we need a $SWAP$ and a Hadamard (H) gate both contained in C_2 . Since some graph states can directly implement Clifford gates with Pauli measurements only, we first get rid of all CCZ hyperedges from the resource state by measuring all remaining boxes in Fig. 4 (b) in Pauli- X bases resulting to the state in Fig. 6 (b) (the full Pauli- X measurement rule is needed for the derivation) and looking at the bigger fragment, we get a graph as in Fig. 6 (c). The main idea here is to get rid of all the vertices which might be included in edges corresponding to byproduct CZ 's. Then, we make Pauli- Z measurements (qubits to which an H is applied, we measure in the Pauli- X basis) on colored vertices. As a result, we project to a hexagonal lattice deterministically. The hexagonal lattice can implement any Clifford gate in parallel up to $\{X, Z\}$ byproducts using Pauli measurements only [42], and therefore, we can implement a $SWAP$ gate. The $SWAP$ and CCZ^{nn} gates together give a CCZ gate over arbitrary distance, up to $\{CZ, X, Z\}$ byproducts.

Finally, after every CCZ gate layer, we need to implement the Hadamard layer, which itself is an easy task [26]. However, since Hadamard gates do not commute with CZ byproducts appearing in the implementation of CCZ 's, we need to correct all CZ 's. We can again use the hexagonal lattice to perform the correction step, however, the $(k-1)$ -th correction step as enumerated in Fig. 1 itself introduces $\{X, Z\}$ byproducts which due

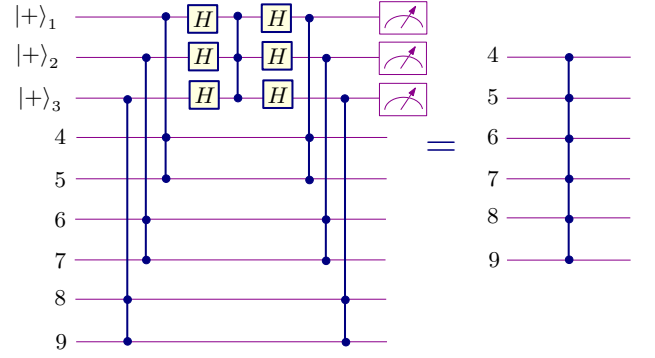


FIG. 7. The circuit identity to create a C^6Z gate. The first three qubits are measured in the X basis. The adaptation of measurement bases is needed twice for two Hadamard layers.

to the commutation relation, $C_{abc}X_a = X_aC_{abc}C_{bc}$, introduces new CZ byproducts before the k -th correction step. Consequently, the measurement results during the $(k-1)$ -th correction must be taken into account to correct all CZ byproducts before the k -th correction step. To sum up, we can parallelize all CCZ gates, but we need to increment the circuit depth for each Hadamard layer in order to correct all CZ byproducts *adaptively*.

Application of parallelization.— Our MBQC inspires a potentially exponentially efficient parallelization of gates, compared to a conventional gate synthesis [32]. Here we discuss the $C^N Z$ gate as an example, and derive the gate identity for implementing $C^N Z$ gate by decomposing it into only CCZ and Hadamard gates, trying to minimize number of Hadamard layers.

Theorem 2. *An N -times Controlled-Z ($C^N Z$) gate can be implemented in $O(\log N)$ logical depth, using $(2N-5)$ CCZ gates and $(N-3)$ ancilla qubits.*

The detailed derivation of the gate identity is given in the Appendix. We create a $C^N Z$ gate iteratively. In Fig. 7 we give the procedure for $N=6$ with only two Hadamard layers in the circuit. Having created the $C^6 Z$ gate, we concatenate the same procedure of applying Hadamard gates and CCZ gates in order to obtain a $C^{12} Z$ gate with only two additional Hadamard layers (see Fig. 11 in the Appendix). Iterating this procedure for implementing a $C^{3 \cdot 2^r} Z$ gate, we need $2r$ layers of Hadamards only. Going back to our proposed resource state, all CCZ gates used in the circuit can be implemented in parallel, and therefore the depth of the computation for $C^N Z$ is $O(\log N)$. Additionally, the number of ancilla qubits in the circuit is $N-3$ and the number of CCZ gates is twice as many as ancilla qubits plus one, therefore, $2N-5$.

In order to highlight that our circuit identity is versatile and of independent interest, we compare it to the standard cluster-state MBQC model [26]. The depth of the circuit implementing a $C^N Z$ gate can be made constant in N on a cluster state if the number of ancilla

qubits is allowed to be $2^N - 1$, namely exponential in the size of the implemented gate. If our circuit from Theorem 2 is adapted on a cluster state, the depth of the circuit increases to logarithmic in N , but at the same time number of ancilla qubits needed decreases to $N - 3$ (see Appendix). In this way our circuit illustrates the trade-off between the space and time required for implementing a quantum circuit, using MBQC.

Summary and outlook.— We introduced a deterministic scheme of MBQC for the gate set of CCZ and H gates, using a three-uniform hypergraph state and Pauli measurements. Our physical implementation enables us to parallelize massively all long-range CCZ gates and the computational depth grows as we change computational bases. To take a broader perspective, one can define the Fourier hierarchy (FH) [4, 6, 7] in terms of the number of the global change of the bases (namely, the globally parallel application of the Hadamard gates). When we consider a polynomial number of gates, notably classical polynomial-time computation, called the complexity class P, belongs to the 0th-level of FH. Since it is known that several important quantum algorithms, such

as Kitaev’s phase estimation, belong to the 2nd-level of FH (which requires only two layers of global Hadamard gates) [7], it would be interesting to explore the implementations of low-level FH algorithms in our formulation. The recent major result by Bravyi et al. [43] which proved quantum exponential advantage in the 2D Hidden Linear Function problem using a shallow circuit in the 2nd-level of FH is really encouraging towards this research direction (see e.g., [44–46]).

We would like to thank D. Orsucci and J. Miller for scientific discussions, and D.-S. Wang for introducing to us his deterministic teleportation protocol using the five-qubit three-uniform hypergraph state in Fig. 8 of the Appendix. M.G. would like to thank A. Miyake, O. Gühne, and G. Cordova for making her visit in Albuquerque possible, and the entire CQuIC group at UNM for hospitality. M.G. and O.G. acknowledge financial support from the DFG and the ERC (Consolidator Grant 683107/TempoQ). M.G. acknowledges funding from the Gesellschaft der Freunde und Förderer der Universität Siegen. A.M. is supported in part by National Science Foundation grants PHY-1521016 and PHY-1620651.

APPENDIX A: THE PAULI- X MEASUREMENT RULE FOR HYPERGRAPH STATES

In this section we derive the Pauli- X measurement rule for hypergraph states. We give a sufficient criterion for the Pauli- X measurements on a hypergraph state to project on a post-measurement state which is local unitary equivalent to some other hypergraph state. This criteria entirely captures the rule for graph states. For formulating the criterion we introduce a term which can be regarded as a generalization of the term neighbourhood known in graph theory. We call it *adjacency* of a vertex $a \in V$ and denote it by $\mathcal{A}(a) = \{e - \{a\} | e \in E \text{ with } a \in e\}$.

Definition 3. *Given a hypergraph state $|H\rangle$ corresponding to a hypergraph $H = (V, E)$. If we write this hypergraph state as follows,*

$$|H\rangle = \frac{1}{\sqrt{2}}|0\rangle_a|H_0\rangle + \frac{1}{\sqrt{2}}|1\rangle_a|H_1\rangle, \quad (2)$$

we say that hypergraph state is expanded over a vertex $a \in V$. By definition $|H_0\rangle$ and $|H_1\rangle$ are also hypergraph states respectively corresponding to hypergraphs H_0 and H_1 with hyperedges $E_0 = \{e \in E | a \notin e\}$ and $E_1 = E_0 \cup \mathcal{A}(a)$. If we choose a subset of vertices $V_x \subset V$ instead of a vertex a , we say that hypergraph state is expanded over a set of vertices $V_x \subset V$ and expansion is done iteratively for every vertex in V_x .

For example, if we want to expand the hypergraph state $|H\rangle$ over vertices a and b , we first expand it over a and then we expand hypergraphs $|H_0\rangle$ and $|H_1\rangle$ separately over b resulting in

$$|H\rangle = \frac{1}{\sqrt{2}}|0\rangle_a \left(|0\rangle_b|H_{00}\rangle + |1\rangle_b|H_{01}\rangle \right) + \frac{1}{\sqrt{2}}|1\rangle_a \left(|0\rangle_b|H_{10}\rangle + |1\rangle_b|H_{11}\rangle \right). \quad (3)$$

If the vertex a is measured in computational basis, the post-measurement state is a hypergraph state $|H_0\rangle$ for the outcome 0 or $|H_1\rangle$ for the outcome 1. However, if measured in Pauli- X basis, then the post-measurement state is $\propto (|H_0\rangle \pm |H_1\rangle)$ and is not always local unitary equivalent to a hypergraph state. To check if for a given hypergraph state measuring a vertex a or a set of vertices V_a in Pauli- X basis gives a state local unitary equivalent to a hypergraph state, one can expand an original hypergraph state over a vertex a or a set V_a and check if all possible equally weighted superposition of expanded hypergraph states gives some other hypergraph state or a state which is local unitary equivalent to a hypergraph state.

Let us consider particular cases of hypergraph states $|H\rangle$ which when expanded over three vertices 1, 2, 3, gives eight new hypergraphs satisfying the following constraints $H_{000} = H_{001} = H_{010} = H_{100} \equiv H_a$ and $H_{111} = H_{110} =$

#	Outcome	Post-measurement state
1.	$\langle ++ + _{123}$	$\propto (H_\alpha\rangle + H_\beta\rangle)$
2.	$\langle ++ - _{123}$	$\propto (H_\alpha\rangle - H_\beta\rangle)$
3.	$\langle + - - _{123}$	0
4.	$\langle - - - _{123}$	$\propto -(H_\alpha\rangle - H_\beta\rangle)$

TABLE II. All possible post-measurement states for Pauli- X measurements on qubits 1, 2, 3 in Eq. (4). Case 2 and 4 are equivalent up to a global sign.

$H_{101} = H_{011} \equiv H_\beta$. Then the expanded state can be written as follows:

$$|H\rangle = \frac{1}{\sqrt{8}} \left((|000\rangle + |001\rangle + |010\rangle + |100\rangle)_{123} \otimes |H_\alpha\rangle + (|111\rangle + |110\rangle + |101\rangle + |011\rangle)_{123} \otimes |H_\beta\rangle \right). \quad (4)$$

If qubits 1, 2, 3 are all measured in Pauli- X bases, due to the symmetry of the first three qubits, there are only four possible post measurement states presented in Table II. We see from Table II that outcome $\langle + - - |$ never occurs and outcomes $\langle ++ - |$ and $\langle - - - |$ are equivalent to each other up to the global sign. Therefore, if we measure the first three qubits of the hypergraph state $|H\rangle$ as presented in Eq. (4), there are only two possible post-measurement states and they correspond to the equally weighted superposition of two hypergraph states $|H_\alpha\rangle \pm |H_\beta\rangle$. These three qubits and their adjacencies are of our interest and in the main text they are denoted by a box. Below we consider three examples where we measure these three qubits but we vary the hypergraphs H_α and H_β .

The equally weighted superposition of two hypergraph states is not always a hypergraph state again unless we choose two hypergraphs H_α and H_β specifically. Here we give a sufficient criterion for equally weighted superpositions of two hypergraph states being a hypergraph state up to local unitary operations and derive the graphical rule for such cases:

Theorem 4. Let $H_\alpha = (V, E)$ and $H_\beta = (V, E \cup \{a\} \cup \tilde{E})$, where \tilde{E} are hyperedges not containing a vertex $a \in V$. Then the equally weighted superpositions of two hypergraph states $|H_\alpha\rangle$ and $|H_\beta\rangle$ up to the Hadamard gate acting on the vertex a , H_a are still hypergraph states denoted by $|H_+\rangle$ and $|H_-\rangle$:

$$H_a|H_+\rangle \equiv H_a(|H_\alpha\rangle + |H_\beta\rangle) \propto \prod_{e' \in E'} C_{e'} \prod_{e_a \in \mathcal{A}^\alpha(a)} \prod_{\tilde{e} \in \tilde{E}} C_{e_a \cup \tilde{e}} C_{\tilde{e} \cup a} |+\rangle^{\otimes N}, \quad (5)$$

$$H_a|H_-\rangle \equiv H_a(|H_\alpha\rangle - |H_\beta\rangle) \propto C_a \prod_{e' \in E'} C_{e'} \prod_{e_a \in \mathcal{A}^\alpha(a)} C_{e_a} \prod_{\tilde{e} \in \tilde{E}} C_{e_a \cup \tilde{e}} C_{\tilde{e} \cup a} |+\rangle^{\otimes N}. \quad (6)$$

Here $\mathcal{A}^\alpha(a)$ is the adjacency of the vertex a in hypergraph H_α and $E' = \{e' | a \notin e', e' \in E\}$ and $C_a = Z_a$.

Proof. Let us assume that $a = 1$. Then we get:

$$H_1|H_+\rangle = H_1(|H_\alpha\rangle + |H_\beta\rangle) \quad (7)$$

$$= H_1(|H_\alpha\rangle + Z_1 \prod_{\tilde{e} \in \tilde{E}} C_{\tilde{e}} |H_\alpha\rangle) \quad (8)$$

$$= H_1 \left(\prod_{e \in E} C_e \left(|+\rangle^{\otimes N} + Z_1 \prod_{\tilde{e} \in \tilde{E}} C_{\tilde{e}} |+\rangle^{\otimes N} \right) \right) \quad (9)$$

$$= H_1 \prod_{e \in E} C_e H_1 H_1 \left(\left[|+\rangle + |-\rangle \prod_{\tilde{e} \in \tilde{E}} C_{\tilde{e}} \right] |+\rangle^{\otimes N-1} \right) \quad (10)$$

$$= H_1 \prod_{e' \in E'} C_{e'} \prod_{e'' \in E''} C_{e''} H_1 H_1 \left(\left[|+\rangle + |-\rangle \prod_{\tilde{e} \in \tilde{E}} C_{\tilde{e}} \right] |+\rangle^{\otimes N-1} \right) \quad (11)$$

$$= \prod_{e' \in E'} C_{e'} H_1 \prod_{e'' \in E''} C_{e''} H_1 H_1 \left(\left[|+\rangle + |-\rangle \prod_{\tilde{e} \in \tilde{E}} C_{\tilde{e}} \right] |+\rangle^{\otimes N-1} \right) \quad (12)$$

$$= \prod_{e' \in E'} C_{e'} \prod_{e_1 \in \mathcal{A}^\alpha(1)} CNOT_{e_1, 1} \left(\left[|0\rangle + |1\rangle \prod_{\tilde{e} \in \tilde{E}} C_{\tilde{e}} \right] |+\rangle^{\otimes N-1} \right) \quad (13)$$

$$\propto \prod_{e' \in E'} C_{e'} \prod_{e_1 \in \mathcal{A}^\alpha(1)} CNOT_{e_1,1} \prod_{\tilde{e} \in \tilde{E}} C_{\tilde{e} \cup 1} |+\rangle^{\otimes N} \quad (14)$$

$$= \prod_{e' \in E'} C_{e'} \prod_{e_1 \in \mathcal{A}^\alpha(1)} \prod_{\tilde{e} \in \tilde{E}} C_{e_1 \cup \tilde{e}} C_{\tilde{e} \cup 1} |+\rangle^{\otimes N} \quad (15)$$

In Eq. (10) we decompose a set of hyperedges E into two parts: E' , hyperedges which do not contain the vertex 1 and E'' hyperedges which contain the vertex 1. In Eq. (11) the set of hyperedges $\prod_{e' \in E'} C_{e'}$ commute with H_1 and going to Eq. (12), $H_1 \prod_{e'' \in E''} C_{e''} H_1 = \prod_{e_1 \in \mathcal{A}^\alpha(1)} CNOT_{e_1,1}$, since Hadamard gate H_1 changes Z_1 to X_1 and, therefore, generalized Controlled- Z gates become generalized $CNOT$ gates.

In Eq. (12), H_1 is applied to $|\pm\rangle$ and in Eq. (13) a new hypergraph state is obtained, which is written in an expanded form over vertex 1. If we write this hypergraph state we get Eq. (14):

$$\left(\left[|0\rangle + |1\rangle \prod_{\tilde{e} \in \tilde{E}} C_{\tilde{e}} \right] |+\rangle^{\otimes N-1} \right) \propto \prod_{\tilde{e} \in \tilde{E}} C_{\tilde{e} \cup 1} |+\rangle^{\otimes N}. \quad (16)$$

Then generalized $CNOT$ gates are applied to a new hypergraph state in Eq. (14). The action of generalized $CNOT$ gate was described in Ref. [47] as follows: Applying the generalized $CNOT_{Ct}$ gate to a hypergraph state, where a set of control qubits C controls the target qubit t , introduces or deletes the set of edges $E_t = \{e_t \cup C | e_t \in \mathcal{A}(t)\}$.

In Eq. (14) the generalized $CNOT$ gate is applied to the hypergraph state which corresponds to the hypergraph $(V, \{\tilde{e} \cup \{1\} | \tilde{e} \in \tilde{E}\})$. The target qubit in the generalized $CNOT$ gate is the vertex 1 and its adjacency is, therefore, given by edge-set \tilde{E} . The control qubits are presented by the edge-set $\mathcal{A}^\alpha(1)$, which correspond to the adjacency of the vertex 1 in the hypergraph H_α . The action of generalized $CNOT$ gate takes the pairwise union of hyperedges in $\mathcal{A}^\alpha(1)$ and \tilde{E} and adds or deletes new hyperedges:

$$\prod_{e_1 \in \mathcal{A}^\alpha(1)} \prod_{\tilde{e} \in \tilde{E}} C_{e_1 \cup \tilde{e}}. \quad (17)$$

Inserting these hyperedges in Eq. (15), we get the final hypergraph states:

$$H_1(|H_+\rangle) \propto \prod_{e' \in E'} C_{e'} \prod_{e_1 \in \mathcal{A}^\alpha(1)} \prod_{\tilde{e} \in \tilde{E}} C_{e_1 \cup \tilde{e}} C_{\tilde{e} \cup 1} |+\rangle^{\otimes N}. \quad (18)$$

In case of the minus superposition $H_1|H_-\rangle$, the derivations are very similar to $H_1|H_+\rangle$ up to Eq. (13): In particular, due to the minus sign in the superposition, we get a different hypergraph state from the one in Eq. (16):

$$H_1(|+\rangle - |-\rangle \prod_{\tilde{e} \in \tilde{E}} C_{\tilde{e}}) |+\rangle^{\otimes N-1} = (|0\rangle - |1\rangle \prod_{\tilde{e} \in \tilde{E}} C_{\tilde{e}}) |+\rangle^{\otimes N-1} = C_1 \prod_{\tilde{e} \in \tilde{E}} C_{\tilde{e} \cup 1} |+\rangle^{\otimes N} \quad (19)$$

Now we apply generalized $CNOT$ gate to the hypergraph state in Eq. (19) :

$$\prod_{e_1 \in \mathcal{A}^\alpha(1)} CNOT_{e_1,1} C_1 \prod_{\tilde{e} \in \tilde{E}} C_{\tilde{e} \cup 1} |+\rangle^{\otimes N}. \quad (20)$$

The hypergraph state in Eq. (19) has the additional edge C_1 and this means that the adjacency of the vertex 1 in Eq. (20) is given by the edge-set $\{\tilde{E} \cup \{\emptyset\}\}$. The action of generalized $CNOT$ gate takes the pairwise union of hyperedges in $\mathcal{A}^\alpha(1)$ and $\{\tilde{E} \cup \{\emptyset\}\}$ and introduces new hyperedges of the form in the hypergraph:

$$\prod_{e_1 \in \mathcal{A}^\alpha(1)} C_{e_1} \prod_{\tilde{e} \in \tilde{E}} C_{e_1 \cup \tilde{e}} \quad (21)$$

Inserting these hyperedges in the original derivations, gives us the final hypergraph state:

$$H_1|H_-\rangle \propto C_1 \prod_{e' \in E'} C_{e'} \prod_{e_1 \in \mathcal{A}^\alpha(1)} C_{e_1} \prod_{\tilde{e} \in \tilde{E}} C_{e_1 \cup \tilde{e}} C_{\tilde{e} \cup 1} |+\rangle^{\otimes N}. \quad (22)$$

□

Given any graph state $|G\rangle$ corresponding to a connected graph $G = (V, E)$, if we expand it over any of its vertices $a \in V$,

$$|G\rangle = \frac{1}{\sqrt{2}} \left(|0\rangle_a |G_0\rangle + |1\rangle_a |G_1\rangle \right), \quad (23)$$

then graphs corresponding to $|G_0\rangle$ and $|G_1\rangle$ satisfy the condition of Theorem 4 since $|G_1\rangle = \prod_{i \in \mathcal{N}(a)} Z_i |G_0\rangle$, where $\mathcal{N}(a)$ is the neighbourhood of the vertex a . So, if the vertex a is measured in Pauli- X basis, the post measurement states are the equally weighted superpositions of $|G_0\rangle$ and $|G_1\rangle$ and therefore, Theorem 4 gives the rules for deriving post-measurement states for both outcomes of measurement Pauli- X basis. The rules for Pauli- X measurement for graph states was previously derived in Ref. [41] using a different approach.

EXAMPLES OF PAULI- X MEASUREMENTS ON HYPERGRAPH STATES

Here we give examples of Pauli- X measurements on hypergraph states. In all of our examples exactly three vertices are measured in Pauli- X bases. The post-measurement states are derived by first expanding the hypergraph state over these three vertices as shown in Eq.(4), then checking if new emerging hypergraphs H_α and H_β satisfy the condition of Theorem 4. And only the final step is to apply the result of Theorem 4 to give the post-measurement hypergraph states.

Here we only consider three-uniform hypergraph states and focus on cases when post-measurement states are graph states regardless of the measurement outcomes, in general this is not the case.

Example 1: The smallest three-uniform hypergraph state which after measuring the first three qubits in Pauli- X basis can deterministically project on a Bell state is (see Fig. 8) :

$$|H_5\rangle = C_{124}C_{125}C_{134}C_{135}C_{234}C_{235}|+\rangle^{\otimes 5} = \frac{1}{2\sqrt{2}} \left((|000\rangle + |001\rangle + |010\rangle + |100\rangle)|+\rangle^{\otimes 2} + (|011\rangle + |110\rangle + |101\rangle + |111\rangle)|-\rangle^{\otimes 2} \right). \quad (24)$$

The state $|H_5\rangle$ is given in the expanded form over vertices 1, 2, 3 as in Eq. (4) and $|H_\alpha\rangle = |+\rangle^{\otimes 2}$ and $|H_\beta\rangle = |-\rangle^{\otimes 2} = Z^{\otimes 2}|+\rangle^{\otimes 2}$.

We fix a to be vertex 4, H_α to have hyperedges $E_\alpha = \{\}$ and H_β to have hyperedges $E_\beta = \{\{4\} \cup \tilde{E}\}$, where $\tilde{E} = \{\{5\}\}$. These two hypergraphs satisfy condition of Theorem 4. So, measuring qubits 1, 2, 3 in Pauli- X basis gives two possible post-measurement hypergraph states $H_4|H_+\rangle \propto |+\rangle^{\otimes 2} + |-\rangle^{\otimes 2}$ with the probability 1/5 and $H_4|H_-\rangle \propto |+\rangle^{\otimes 2} + |-\rangle^{\otimes 2}$ with the probability 4/5. Using Theorem 4 we derive these post-measurement states:

$$H_4|H_+\rangle \propto H_4 \left(|+\rangle^{\otimes 2} + |-\rangle^{\otimes 2} \right) \propto C_{45}|+\rangle^{\otimes 2} \quad \text{and} \quad H_4|H_-\rangle \propto H_4 \left(|+\rangle^{\otimes 2} - |-\rangle^{\otimes 2} \right) \propto C_{45}C_4|+\rangle^{\otimes 2}. \quad (25)$$

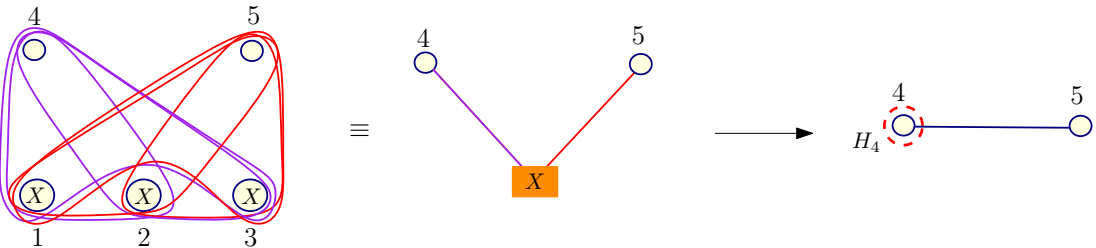


FIG. 8. The five-qubit three-uniform hypergraph state [48] is the smallest hypergraph state with no usual graph edges which can project on a Bell state deterministically. It has hyperedges $E = \{\{1, 2, 4\}, \{1, 2, 5\}, \{1, 3, 4\}, \{1, 3, 5\}, \{2, 3, 4\}, \{2, 3, 5\}\}$. The qubits 1, 2, 3 are measured in X -basis and the post-measurement state is a graph state with a Hadamard correction on the vertex 4. The graph state is obtained with unit probability but up to Pauli- Z_4 byproduct. The probabilistic Pauli- Z_4 is denoted by the dotted circle and it appears with the probability 4/5 when the product of Pauli- X measurement outcomes is -1 .

Example 2: Let us consider the six-qubit hypergraph state $|H_6\rangle$ presented on Fig. 3 (a). After measuring qubits 1, 2, 3 in X -basis we project on the three-qubit graph state. To see this, we write $|H_6\rangle$ directly in the expanded form over vertices 1, 2, 3:

$$\begin{aligned} |H_6\rangle \propto & (|000\rangle + |001\rangle + |010\rangle + |100\rangle) \otimes \begin{array}{ccc} 4 \bullet & 5 \bullet & 6 \bullet \end{array} \\ & + (|110\rangle + |101\rangle + |011\rangle + |111\rangle) \otimes \begin{array}{ccc} 4 \circ & 5 \circ & 6 \circ \end{array}. \end{aligned} \quad (26)$$

Here H_α has hyperedges $E_\alpha = \{\}$ and H_β has hyperedges $E_\beta = \{\{4\}, \{5\}, \{6\}\}$ and we fix to apply the Hadamard correction on the vertex $a = 5$. We can use Theorem 4 to derive two post-measurement states upto Hadamard gate applied to the vertex 5:

$$H_5|H_+\rangle \propto C_{45}C_{56}|+\rangle^{\otimes 3} \quad \text{and} \quad H_5|H_-\rangle \propto C_{45}C_{56}C_5|+\rangle^{\otimes 3}. \quad (27)$$

Example 3: Let us consider more complicated six-qubit hypergraph state $|H_6\rangle$ presented on Fig. 3 (b). We write this state expanded over vertices 1, 2, 3:

$$\begin{aligned} |H_6\rangle \propto & (|000\rangle + |001\rangle + |010\rangle + |100\rangle) \otimes \begin{array}{ccc} 4 \bullet & 5 \bullet & 6 \bullet \end{array} \\ & + (|110\rangle + |101\rangle + |011\rangle + |111\rangle) \otimes \begin{array}{ccc} 4 \circ & 5 \circ & 6 \circ \end{array}. \end{aligned} \quad (28)$$

Here H_α has hyperedges $E_\alpha = \{\{1, 2, 3\}\}$ and H_β has hyperedges $E_\beta = \{\{1, 2, 3\}, \{4\}, \{5\}, \{6\}\}$ and we fix to apply the Hadamard correction on the vertex $a = 5$. We can use Theorem 4 to derive two post-measurement states upto Hadamard gate applied to qubit 5:

$$H_5|H_+\rangle \propto C_{45}C_{56}|+\rangle^{\otimes 3} \quad \text{and} \quad H_5|H_-\rangle \propto C_{45}C_{56}C_{46}C_5|+\rangle^{\otimes 3}. \quad (29)$$

Remark. We can increase the number of vertices that we measure in Pauli- X and generalize a notion of the box defined in the main text. The box that we considered up to now was corresponding to the structure of the expanded three vertices and was always connected to the rest of the hypergraph with three-qubit hyperedges. Now we try to extend this result to higher cardinality edges. Let us expand a hypergraph state over m -qubits, where $3 \leq m \leq N - 2$ is an odd number, in the following way:

$$|H_N\rangle \propto \left(\sum_x |x\rangle \right) \otimes |H_\alpha\rangle + \left(\sum_y |y\rangle \right) \otimes |H_\beta\rangle, \quad (30)$$

where $x, y \in \{0, 1\}^m$ and the first sum runs over all computational bases elements with the weight $w(x) \leq \lfloor m/2 \rfloor$ and the second sum runs over all computational bases elements with the weight $w(y) > \lfloor m/2 \rfloor$.

If all the first m vertices are measured in Pauli- X bases, then we again get two possible measurement outcomes $|H_\alpha\rangle \pm |H_\beta\rangle$. However, the box now can look very different from the $m = 3$ case.

For simplicity let us fix $|H_\alpha\rangle = |+\rangle^{\otimes \lfloor N-m \rfloor}$ and $|H_\beta\rangle = |-\rangle^{\otimes \lfloor N-m \rfloor}$. The smallest hyperedge the new type of a box is connected to the rest of the hypergraph has a cardinality equal to $\lfloor m/2 \rfloor + 1$. But in addition, for some cases of m with this construction the box will be connected to the rest of the hypergraph with different sizes of hyperedges.

To illustrate this let us consider an example of $|H_7\rangle$, where $m = 5$ and $|H_\alpha\rangle = |+\rangle^{\otimes 2}$ and $|H_\beta\rangle = |-\rangle^{\otimes 2}$. Then the smallest cardinality hyperedge in the hypergraph is of a size four - the smallest weight of vector $|y\rangle$ is equal to $\lceil 5/2 \rceil = 3$ and plus 1. However, these are not all the hyperedges in the hypergraph: The vectors with the weight four are in the second summand and they are tensored with $|-\rangle^{\otimes 2}$. However, if we choose any four vertices among m , then every three from them are connected to both vertices $m+1$ and $m+2$, but $\binom{4}{3} = 4$, which is an even number. So, the hypergraph must have additional cardinality 5 edges. Similarly we have to check the weight of the last term in the sum: $\binom{5}{3} + \binom{5}{4} = 15$ is an odd number and, therefore, there is no cardinality six edges in the hypergraph. Therefore, similarly to $m = 3$ case, we got a box containing five qubits but the box is connected to the rest of the hypergraph with four- and five- qubit hyperedges in a symmetric manner.

APPENDIX B: IMPLEMENTATION OF CCZ^{nn} GATE

Since we have chosen $\{CCZ, H\}$ to be the universal gate set, we need to show in detail how to implement these gates on our resource state. To start with, we implement CCZ gates only on the nearest neighbor qubits (denote it

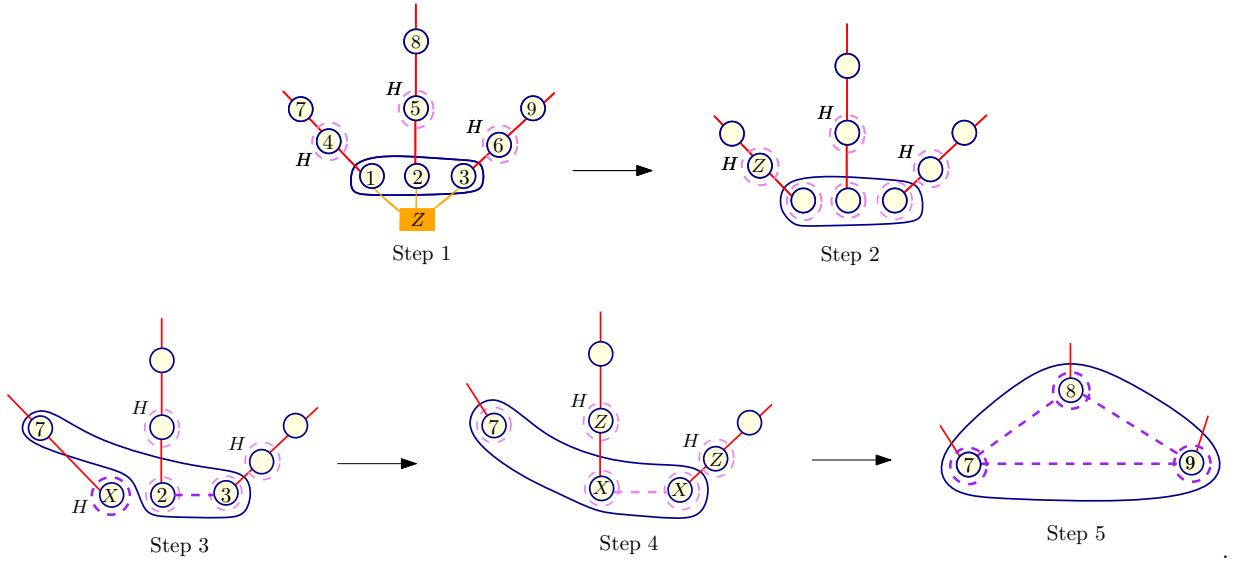


FIG. 9. Implementing CCZ^{nn} gate. All measurements are made simultaneously. We present them step by step to emphasize how CZ byproducts come into the computational scheme. Step 1: Pauli-Z measurement on the box removes the box and introduces Pauli-Z byproducts on vertices 1, 2, 3. Step 2: The vertex 4 is measured in X -basis projecting on the state at step 3. Step 3: We see the CZ_{23} byproduct depending on the outcome of the measurement on the vertex 4. Measuring the vertex 1 in Pauli-Z, projects on the hypergraph at step 4. Step 4: Repeating the measurements for vertices 2, 3, 5, 6 gives the state at step 5.

by CCZ^{nn}) and therefore, we need $SWAP$ gate too. The goal is to implement all the gates deterministically. All Pauli measurements are made in one step but for simplicity we consider them in several steps. At the step one the box is measured in Pauli-Z basis. This evidently removes the box entirely and introduces Pauli-Z byproducts on the vertices 1, 2, 3 as presented on Fig. 9.

On Fig. 9 at step 1 we first describe the measurements needed to get CCZ^{nn} gate using our resource state. Now let us measure the vertex 4 in Pauli-Z basis, this effectively implements Pauli-X measurement, since the Hadamard gate was applied to this vertex. We need to use Theorem 4 to derive a post-measurement state. Let us write the hypergraph state in the expanded form over the vertex 4:

$$|H\rangle = \frac{1}{\sqrt{2}}(|0\rangle_4|H_0\rangle + |1\rangle_4|H_1\rangle) = \frac{1}{\sqrt{2}}(|0\rangle_4|H_0\rangle + |1\rangle_4 Z_1 Z_7 |H_0\rangle). \quad (31)$$

Then $|H_0\rangle$ and $|H_1\rangle$ satisfy the condition of Theorem 4 with a Hadamard applied on the vertex 1 and accordingly the post-measurement state is given on Fig. 9 at step 3. CCZ gate is now applied to the vertices 2, 3, 7. At this step we have to point out that the post-measurement state has the edges $\{1\} \{2, 3\}$ for the measurement outcome " - 1 ". Thus, this is where CZ byproducts come into the computation scheme discussed in the main text. At the step 3 the vertex 1 is measured in Pauli-X basis and since the Hadamard is applied to this qubits, this implements Pauli-Z measurement instead. Repeating this measurement pattern over as shown at the step 4 given the final state at the step 5, where CCZ gate is applied to vertices 7, 8, 9 upto CZ and Z byproducts.

APPENDIX C: DISCUSSION OF THE COMPLEXITY

Here we first give the proof for the gate identity from the main text.

Lemma 5. *The following equality holds for any state $|\psi\rangle$ and sets $i \in e_1$ and $i \in e_2$:*

$$C_{e_1} H_i C_{e_2} H_i C_{e_1} |+\rangle_i |\psi\rangle = |+\rangle_i C_{e_1 \cup e_2 \setminus \{i\}} |\psi\rangle. \quad (32)$$

Proof. Assume that $i = 1$ and denote $e'_1 \equiv e_1 \setminus \{1\}$ and $e'_2 \equiv e_2 \setminus \{1\}$, then $e_1 \cup e_2 \setminus \{1\} = e'_1 \cup e'_2$:

$$C_{e_1} H_i C_{e_2} H_i C_{e_1} |+\rangle_i |\psi\rangle = C_{\{1\} \cup e'_1} CNOT_{e'_2, 1} C_{\{1\} \cup e'_1} |+\rangle_1 |\psi\rangle \quad (33)$$

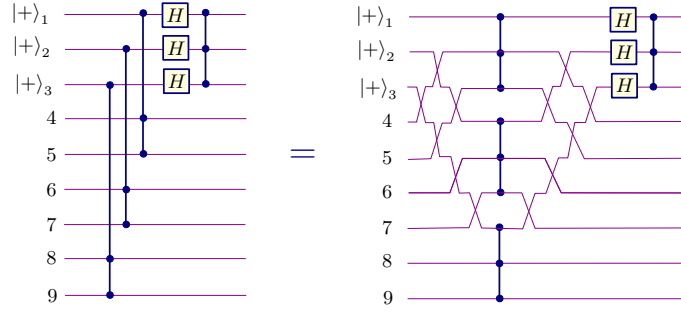


FIG. 10. Decomposing C^6Z gate in nearest neighbor CCZ 's and $SWAP$ gates. Only the first half part of the protocol is presented since the other half is exactly the same. There are 12 $SWAP$ gates on the figure, but to implement C^6Z gate we need totally 24 $SWAP$ gates.

We can express an arbitrary multi-qubit state $|\psi\rangle$ in Pauli- X orthonormal basis $|j\rangle$: $|\psi\rangle = \sum_j \phi_j |j\rangle$. Then each vector $|+\rangle_1 |j\rangle$ is itself a hypergraph state. In Ref. [47] the action of a generalized $CNOT$ gate was described on hypergraph states as we have already used in the previous sections: Applying the generalized $CNOT_{Ct}$ gate to a hypergraph state, where a set of control qubits C controls the target qubit t , introduces or deletes the set of edges $E_t = \{e_t \cup C | e_t \in \mathcal{A}(t)\}$.

In our example the target qubit $t = 1$ and for each hypergraph state $|+\rangle_1 |j\rangle$ the target qubit $t = 1$ is in a single hyperedge C_{e_1} only. Therefore from linearity follows that:

$$C_{\{1\} \cup e'_1} CNOT_{e'_2, 1} C_{\{1\} \cup e'_1} |+\rangle_1 \left(\sum_j \psi_j |j\rangle \right) = C_{\{1\} \cup e'_1} C_{e_2 \cup e'_1} C_{\{1\} \cup e'_1} |+\rangle_1 \left(\sum_j \psi_j |j\rangle \right) = C_{e_2 \cup e'_1} |+\rangle_1 |\psi\rangle \quad (34)$$

□

For an example let us step-by-step consider the circuit in Fig. 7 in the main text implementing a C^6Z gate:

$$C_{145} H_1 C_{123} H_1 C_{145} |+\rangle_1 |+\rangle_2 |+\rangle_3 |\psi\rangle_{456789} = C_{2345} |+\rangle_1 |+\rangle_2 |+\rangle_3 |\psi\rangle_{456789}. \quad (35)$$

Applying the same identity one more time when we have a Hadamard on the second qubit (we omit the first qubit $|+\rangle_1$):

$$C_{267} H_2 C_{2345} H_2 C_{267} |+\rangle_2 |+\rangle_3 |\psi\rangle_{456789} = C_{34567} |+\rangle_2 |+\rangle_3 |\psi\rangle_{456789}. \quad (36)$$

And finally, using the third qubit $|+\rangle_3$ for the same identity, we get the C^6Z gate (we again omit writing $|+\rangle_2$):

$$C_{389} H_3 C_{34567} H_3 C_{389} |+\rangle_3 |\psi\rangle_{456789} = |+\rangle_3 C_{456789} |\psi\rangle_{456789}. \quad (37)$$

Measuring qubits 1, 2, 3 in Pauli- X bases, we get $C_{456789} = C^6Z$ gate being applied to the arbitrary state $|\psi\rangle_{456789}$.

In Fig. 7 in the main text the C^6Z gate is implemented using a particular gate identity. In Fig. 10 (a) we rewrite the first half of the circuit using only CCZ^{nn} and $SWAP$ gates. To implement the entire circuit, there are *seven* CCZ^{nn} , six Hadamard and twenty-four $SWAP$ gates needed. In general, to implement a $C^N Z$ gate with our protocol having already created a $C^{N/2} Z$ gate, we need $N(N-2) \approx N^2$ $SWAP$ gates. So, in order to create $C^N Z$ gate we need to sum up $SWAP$ gates needed at all previous steps of iteration. If $N = 3 \cdot 2^r$, then there are totally $r = \log(N/3)$ iterations in our model from Observation 2. To sum up, totally

$$\sum_{k=1}^r (3 \cdot 2^k)^2 = 9 \sum_{k=1}^r 2^{2k} = 9 \frac{4}{3} (4^r - 1) = \frac{4}{3} (N^2 - 9) \quad (38)$$

$SWAP$ gates are needed.

Next we look into the standard protocol for creating the $C^N Z$ gate using MBQC. In Ref. [26] the 55-qubit cluster state is given to implement three-qubit phase-gates. Some of the vertices are missing from the cluster as they have been measured in Pauli- Z basis (see Fig. 12 (a) for the 55-qubit cluster state from Ref. [26]). The gray qubits serve for input and output registers. The main idea of the protocol is to measure all the vertices displayed on Fig. 12 (a) except

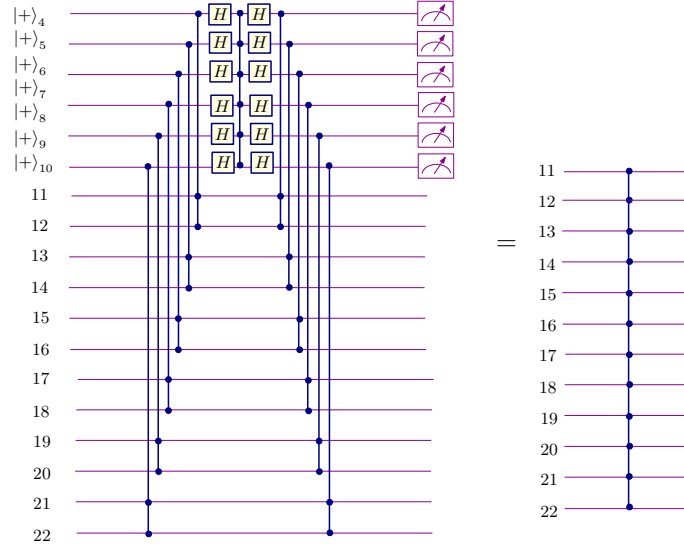


FIG. 11. The circuit identity implementing $C^{12}Z$ gate. Here the middle C^6Z gate was created with the circuit on Fig. 7. The procedure can be iterated to general $C^N Z$ gate.

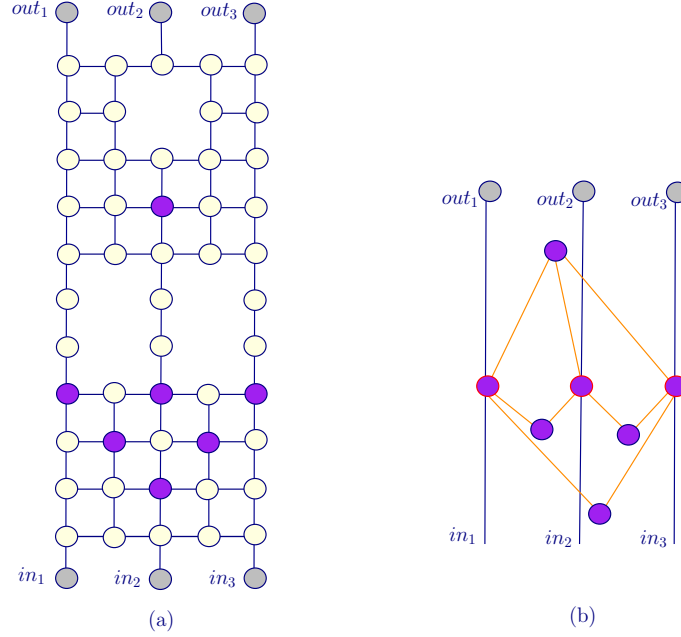


FIG. 12. (a) The 55-qubit graph state given in Ref. [26], which can implement three-qubit phase-gates. Six gray vertices are for input-output, seven dark purple vertices are measured in the second round of measurement, the rest is measured in Pauli- X basis in the first round and the vertices which are already removed are measured in Pauli- Z basis. (b) The seven-qubit graph state obtained after Pauli measurements on (a) capable of implementing a three-qubit phase-gates [26, 49].

the dark purple ones in the first round of measurements in Pauli- X basis simultaneously. Resulting post-measurement state up to Pauli- Z byproducts is the seven-qubit graph state on Fig. 12 (b). Note the similarity of this graph with the graph in Fig. 5 of Ref. [49]

We draw this graph state in the following way: The graph has $\binom{3}{1} = 3$ central vertices, which are connected to input-output wires, $\binom{3}{3} = 1$ vertex adjacent to all the central qubits, and $\binom{3}{2} = 3$ vertices, each adjacent to only two of the central vertices such that all pairs from the central vertices are connected to distinct vertices. Totally, this makes $\binom{3}{1} + \binom{3}{2} + \binom{3}{3} = 2^3 - 1 = 7$ qubits. Then, depending on the previous Pauli- X measurement outcomes, each of these seven qubits are measured in the two eigenbases of $U_Z(\pm\frac{\pi}{4})XU_Z(\pm\frac{\pi}{4})^\dagger$ creating a three-qubit phase-gate up to Pauli byproducts [26, 49].

If we extend this result for C^4Z gate, the initial cluster state must be reduced to the graph state via Pauli measurements implemented in parallel. The structure of this graph is analogous to the one discussed for C^3Z case. But now we need $\sum_{i=1}^4 \binom{4}{i} = 2^4 - 1$ qubits. From here one can see that to implement a $C^N Z$ gate in the standard way starting from the cluster state, one would only need to adapt measurement basis twice, which is constant for any N , but number of qubits one would require is $\sum_{i=1}^N \binom{N}{i} = 2^N - 1$ which is exponential with the size of the gate implemented [49].

-
- [1] M. Nielsen and I. Chuang, *Quantum Computation and Quantum Information*, Cambridge University Press (2000).
- [2] Y. Shi, *Quantum Inf. Comput.* **3**, 84 (2003).
- [3] D. Aharonov, arXiv:quant-ph/0301040 (2003).
- [4] Y. Shi, *Theor. Computer Science* **344**, 335 (2005).
- [5] C.M. Dawson, H.L. Haselgrove, A.P. Hines, D. Mortimer, M.A. Nielsen, and T.J. Osborne, *Quantum Inf. Comput.* **5**, 102 (2005).
- [6] D. Shepherd, arXiv:quant-ph/0508153 (2006).
- [7] D. Shepherd, *Quantum Complexity: restrictions on algorithms and architectures* (Ph.D. thesis, University of Bristol), Chapter 4, The Fourier Hierarchy, arXiv:1005.1425 (2010).
- [8] A. Montanaro, arXiv:1607.08473 (2016).
- [9] A. Paetzniack and B.W. Reichardt, *Phys. Rev. Lett.* **111**, 090505 (2013).
- [10] A. Kubica, B. Yoshida, and F. Pastawski, *New J. Phys.* **17**, 083026 (2015).
- [11] B. Yoshida, *Phys. Rev. B* **93**, 155131 (2016).
- [12] B. Yoshida, *Ann. Phys.* **337**, 387 (2017).
- [13] T.J. Yoder, arXiv:1705.01686 (2017).
- [14] M. Vasmer and D. Browne, arXiv:1801.04255 (2018).
- [15] R. Qu, J. Wang, Z. S. Li, and Y. R. Bao, *Phys. Rev. A* **87**, 022311 (2013).
- [16] M. Rossi, M. Huber, D. Bruß, and C. Macchiavello, *New J. Phys.* **15**, 113022 (2013).
- [17] O. Gühne, M. Cuquet, F.E.S. Steinhoff, T. Moroder, M. Rossi, D. Bruß, B. Kraus, and C. Macchiavello, *J. Phys. A: Math. Theor.* **47**, 335303 (2014).
- [18] T. Morimae, Y. Takeuchi, and M. Hayashi, *Phys. Rev. A* **96**, 062321 (2017).
- [19] D. W. Lyons, N. P. Gibbons, M. A. Peters, D. J. Upchurch, S. N. Walck, and E. W. Wertz, *J. Phys. A: Math. Theor.* **50**, 245303 (2017).
- [20] M. Rossi, D. Bruß, and C. Macchiavello, *Phys. Scr. T* **160**, 014036 (2014).
- [21] M. Gachechiladze, C. Budroni, and O. Gühne, *Phys. Rev. Lett.* **116**, 070401 (2016).
- [22] J. Miller and A. Miyake, *npj Quantum Information* **2**, 16036 (2016).
- [23] J. Miller and A. Miyake, *Phys. Rev. Lett.* **120**, 170503 (2018).
- [24] X. Chen, Z.-C. Gu, Z.-X. Liu, and X.-G. Wen, *Phys. Rev. B* **87**, 155114 (2013).
- [25] R. Raussendorf and H. J. Briegel, *Phys. Rev. Lett.* **86**, 5188 (2001).
- [26] R. Raussendorf, D. E. Browne, and H. J. Briegel, *Phys. Rev. A* **68**, 022312 (2003).
- [27] H. J. Briegel and R. Raussendorf, *Phys. Rev. Lett.* **86**, 910 (2001).
- [28] D. Gross and J. Eisert, *Phys. Rev. Lett.* **98**, 220503 (2007).
- [29] D. Gross, J. Eisert, N. Schuch, and D. Pérez-García, *Phys. Rev. A* **76**, 052315 (2007).
- [30] D. Gross and J. Eisert, *Phys. Rev. A* **82**, 040303(R) (2010).
- [31] K. Mølmer, L. Isenhower, and M. Saffman, *J. Phys. B* **44**, 184016 (2011).
- [32] D. Maslov, *Phys. Rev. A* **93**, 022311 (2016).
- [33] F. Motzoi, M.P. Kaicher, and F.K. Wilhelm, *Phys. Rev. Lett.* **119**, 160503 (2017).
- [34] T. Monz, K. Kim, W. Hänsel, M. Riebe, A. S. Villar, P. Schindler, M. Chwalla, M. Hennrich, and R. Blatt, *Phys. Rev. Lett.* **102**, 040501 (2009).
- [35] B. P. Lanyon, M. Barbieri, M. P. Almeida, T. Jennewein, T. C. Ralph, K. J. Resch, G. J. Pryde, J. L. O'Brien, A. Gilchrist, and A. G. White, *Nat. Phys.* **5**, 134 (2009).
- [36] A. Fedorov, L. Steffen, M. Baur, M.P. da Silva, and A. Wallraff, *Nature* **481**, 170 (2012).
- [37] D. Gottesman and I. L. Chuang, *Nature* **402**, 390 (1999).
- [38] D. Gottesman, talk at International Conference on Group Theoretic Methods in Physics (1998), arXiv:quant-ph/9807006.
- [39] C. Moore and M. Nilsson, *SIAM J. Comput.* **31**, 799 (2001).
- [40] B. Terhal and D.P. DiVincenzo, *Quantum Inf. Comp.* **4**, 134 (2004).
- [41] M. Hein, W. Dür, J. Eisert, R. Raussendorf, M. Van den Nest, and H.-J. Briegel, *Entanglement in Graph States and its Applications in: Quantum Computers, Algorithms and Chaos*, edited by G. Casati, D.L. Shepelyansky, P. Zoller, and G. Benenti (IOS Press, Amsterdam), arXiv:quant-ph/0602096 (2006).
- [42] M. Van den Nest, A. Miyake, W. Dür, and H. J. Briegel, *Phys. Rev. Lett.* **97**, 150504 (2006).
- [43] S. Bravyi, D. Gosset, and R. König, arXiv:1704.00690 (2017).
- [44] M.J. Bremner, A. Montanaro, and D.J. Shepherd, *Phys. Rev. Lett.* **117**, 080501 (2016).
- [45] M.J. Bremner, A. Montanaro, and D.J. Shepherd, *Quantum* **1**, 8 (2017).
- [46] T. Morimae, Y. Takeuchi, and H. Nishimura, arXiv:1711.10605 (2017).
- [47] M. Gachechiladze, N. Tsimakuridze, and O. Gühne, *J. Phys. A: Math. Theor.* **50**, 19LT01 (2017).
- [48] D.-S. Wang, private communication. The five-qubit three uniform hypergraph state (see Fig. 8 in the Appendix), which allows a projection to a Bell state deterministically, was presented at the 2nd UBC Workshop on Algebraic Structures in Quantum Computation in May 2017.
- [49] N. Tsimakuridze and O. Gühne, *J. Phys. A: Math. Theor.* **50**, 195302 (2017).